

## ACCURATE MODELING OF MICROSTRIP DUMBBELL SHAPED SLOT RESONATOR (DSSR) FOR MINIATURIZED TUNABLE RESONATOR AND BAND-PASS FILTER

D.-J. Jung\* and K. Chang

Department of Electrical and Computer Engineering, Texas A&M University, College Station 77843-3128, USA

**Abstract**—In this paper, a novel dumbbell shaped slot resonator (DSSR) is introduced and investigated based on a circuit theory and electromagnetic (EM) simulation. Lumped and distributed equivalent circuit models are then presented for an analysis of the proposed DSSR. The circuit and EM simulated results validate the DSSR's equivalent circuit models and their analysis methodologies. Since the proposed DSSR does not employ ground slots, additional etching process for the ground plane is not necessary. Thus, one can minimize the cost and fabrication errors. For the DSSR's applications, the miniaturized tunable DSSR and band-pass filter (BPF) are designed, simulated, and measured. The tunable DSSR does not require additional lumped DC-block capacitors since DC is isolated due to the coupled gap structures in an input and output. In the BPF design, two DSSRs are simply coupled by input/output ports. Both simulated and measured results of the designed tunable resonator and BPF show good agreement.

### 1. INTRODUCTION

Many RF and microwave components utilizing slots in the ground plane have been reported in [1–10] for the compact circuit dimensions and harmonic suppression purpose. The lumped equivalent circuit models of these structures, known as a defected ground structure (DGS), are a parallel  $LC$  resonator in series. Since the equivalent circuit model of the DGS is the parallel  $LC$  resonator and it shows a band-stop characteristic in the frequency response, it is difficult to design a band-pass filter (BPF) using only the DGS without additional

---

*Received 17 July 2011, Accepted 8 August 2011, Scheduled 12 August 2011*

\* Corresponding author: Dong-Jin Jung (dongjin3558@neo.tamu.edu).

circuit elements. As shown in [11] and [12], the BPF designs using the DGS should employ other BPF circuit elements in order to produce a frequency pass-band. As a result, their analysis and designs are more difficult due to the complicated circuit structures with the ground slots.

In this paper, the microstrip dumbbell shaped slot resonator (DSSR) and its accurate modeling technique are presented. As the DSSR's applications, the miniaturized tunable resonator and BPF are designed, simulated, and measured. Their equivalent circuit models are also introduced and validated from circuit and EM simulation. Since the designed BPF does not include the ground slots, it is simple in the structure. The designed tunable DSSR using a varactor diode employs a coupled gap structure in input/output ports. Thus, DC is isolated from the RF ports. As a result, lumped DC block capacitors are not necessary for the DC and RF isolation. For the tunable resonator, the DSSR is designed at 6 GHz. Then, the varactor diode, which is MA46600 from M/A-COM, is mounted on the designed DSSR. The simulated and measured results of the miniaturized tunable DSSR validate its equivalent circuit model and the DSSR's analysis methodology. The microstrip miniaturized BPF at the center frequency of 5.8 GHz is designed using two coupled DSSRs and one center line. Therefore, the BPF design can be simple and compact. Since the proposed DSSR does not utilize the slotted ground structures, the design and fabrication are easier than the conventional dumbbell shaped DGS circuits.

The paper is organized as follows. Section 2 presents the DSSR's fundamental characteristics and its equivalent circuit models. The equivalent circuit models are validated from the circuit and EM simulated results. Section 3 discusses the miniaturized tunable DSSR and its equivalent circuit model. In Section 4, the miniaturized BPF design using two coupled DSSRs is presented. In the design, a low dielectric constant substrate has been used to minimize the dielectric loading effects on miniaturization. All circuits in the paper are fabricated on Rogers 5880 with a substrate thickness of 0.508 mm and a dielectric constant of 2.2, and they are measured using an HP 8510 vector network analyzer.

## 2. DUMBBELL SHAPED SLOT RESONATOR (DSSR)

Figure 1 presents the proposed microstrip DSSR. Two square slots ( $D \times D$ ) are connected with a rectangle slot ( $G \times W$ ) on the top plane. The input/output microstrip line widths ( $W$ ) are set to 50 ohm line impedance. Figure 2 shows the top view of the DSSR and its lumped equivalent circuit model. In Figure 2(a), the regions,  $A$  ( $A'$ )

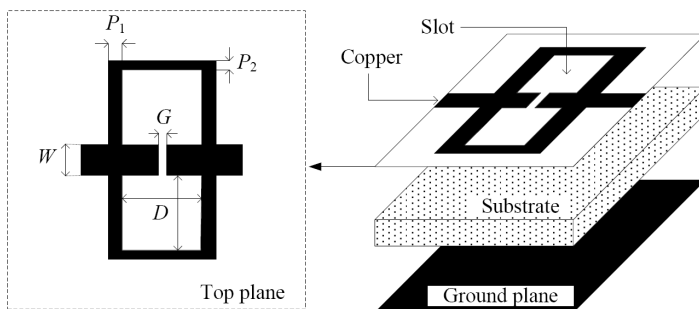


**Figure 1.** Proposed dumbbell shaped slot resonator (DSSR) and its microstrip circuit configuration.

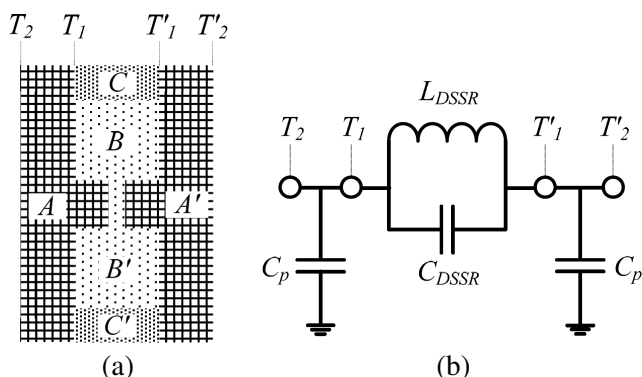


**Figure 2.** Proposed DSSR; (a) top view of the DSSR with divided sections ( $A$ ,  $B$ , and  $C$ ) and (b) lumped equivalent circuit model.

and  $C$  ( $C'$ ), are a copper and the region,  $B$  ( $B'$ ), represents the slot. The microstrip dimensions,  $A$  ( $A'$ ), produce a parallel plate capacitance which is the parallel shunt capacitor ( $C_p$ ) placed at each side of the parallel  $LC$  resonator in Figure 2(b). The capacitor ( $C_{DSSR}$ ) in the parallel  $LC$  resonator is obtained from the cross coupling separated by the gap dimensions ( $G$ ) in Figure 1. The regions,  $B$  ( $B'$ ) and  $C$  ( $C'$ ), are related to the inductance ( $L_{DSSR}$ ) of the center parallel  $LC$  resonator. From EM simulation, it has been found that the current below the cutoff frequency flows around the slot regions,  $B$  ( $B'$ ). Thus, in Figure 1 the wider slot dimensions ( $D \times D$ ) produce the bigger  $L_{DSSR}$ , and the narrower  $P_1$  and  $P_2$  also increase  $L_{DSSR}$ . However, it is difficult to determine the exact  $L_{DSSR}$  value from the given DSSR dimensions. In order to extract the DSSR's element values,  $C_{DSSR}$

should first be found since its exact value can be determined from the cross coupled line's gap capacitance modeling.  $C_P$  value can also be estimated using (1) [13], where  $H$  and  $W$  are the substrate thickness and microstrip dimension, respectively. Once these values are found,  $L_{DSSR}$  can simply be determined by matching the circuit simulated  $S$ -parameters to the EM simulated one.

$$C_P = \varepsilon_o \left[ \left( \frac{\varepsilon_r W}{H} \right)^{1.08} + \left[ \pi (\varepsilon_r + 1) \left\{ \frac{1}{\ln \left( \frac{8H}{W} + 1 \right)} - \frac{W}{8H} \right\} \right]^{1.08} \right]^{1/1.08} \quad (1)$$

For the given DSSR dimensions of  $D = 4.5$ ,  $G = 0.4$ ,  $P_1 = 1.5$ ,  $P_2 = 0.7$ , and  $W = 1.56$  mm,  $C_{DSSR}$  and  $C_P$  are calculated as 0.014 pF and 0.72 pF, respectively. Based on these calculated  $C_{DSSR}$  and  $C_P$ ,  $L_{DSSR}$  is approximately determined by matching the circuit simulated  $S$ -parameters to the EM simulated one. In this process, only except for the exact  $C_{DSSR}$  value,  $L_{DSSR}$  and  $C_P$  values can further be optimized to fit the pass-band return loss, resonant pole, and cutoff frequency. As a result, the optimized  $L_{DSSR}$  and  $C_P$  are found as 1 pF and 1.37 nH, respectively.

Since the DSSR does not employ the ground slot, its equivalent circuit can also be represented using a distributed model. Figures 3(a) and (b) illustrate the proposed DSSR and its distributed equivalent circuit model.  $C_{DSSR}$  for the various coupled gap dimensions can be found from Figure 4. The lumped/distributed equivalent circuit simulation results are compared with its EM simulated  $S$ -parameters in Figure 5. Both circuit and EM simulated results show good agreement in the pass-band return loss, resonant pole, and cutoff frequency. Thus,

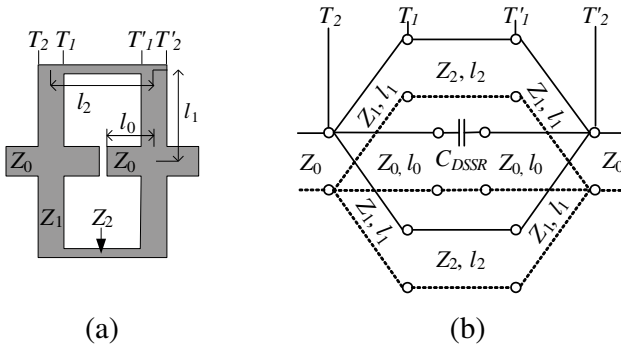


**Figure 3.** Proposed DSSR; (a) top view of the DSSR with impedance notations and (b) distributed equivalent circuit model.

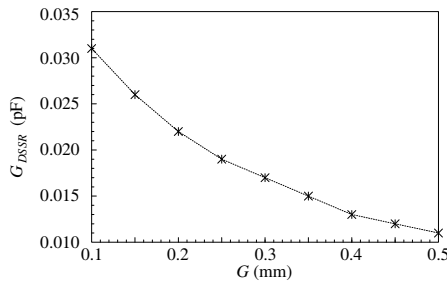


**Figure 4.** Cross coupled capacitance ( $C_{DSSR}$ ) versus the gap dimensions ( $G$ ).

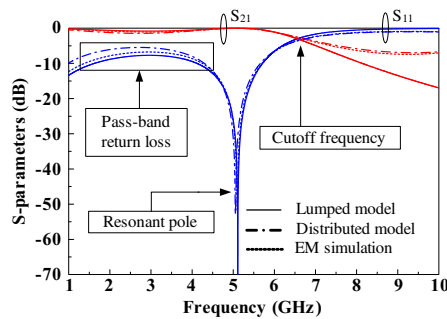


**Figure 5.** Circuit and EM simulated results of the DSSR ( $D = 4.5$ ,  $G = 0.4$ ,  $P_1 = 1.5$ ,  $P_2 = 0.7$ , and  $W = 1.56$  mm), where  $C_{DSSR} = 0.014$  pF,  $L_{DSSR} = 1.37$  nH, and  $C_P = 1$  pF.

the lumped and distributed equivalent circuit models in Figures 2(b) and 3(b) are validated.

Figures 6(a) and (b) present the microstrip coupled DSSR ( $D = 4.5$ ,  $G_1 = 0.4$ ,  $G_2 = 0.2$ ,  $P_1 = 1.5$ ,  $P_2 = 0.7$ ,  $P_3 = 0.6$ , and  $W = 1.56$  mm) and its lumped equivalent circuit model, respectively. Since the DSSR dimensions are the same as the previous DSSR in Figure 5,  $C_{DSSR}$ ,  $L_{DSSR}$ , and  $C_P$  can be expected as the same as 0.014 pF, 1.37 nH, and 1 pF, respectively. In order to determine the series capacitance ( $C_S$ ), the initial lumped element values ( $C_{DSSR} = 0.014$  pF,  $L_{DSSR} = 1.37$  nH, and  $C_P = 1$  pF) of the DSSR are used for the circuit simulation, where  $C_S$  is determined as the value which produces the same bandwidth obtained from the EM simulated one. It should be noted that the pass-band bandwidth of the equivalent circuit model in Figure 6(b) is dominantly affected by the series capacitance ( $C_S$ ). Thus,  $C_S$  can simply be found as 0.14 pF. One other important

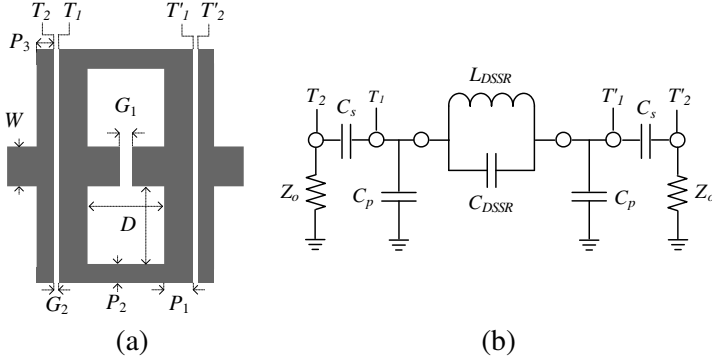


**Figure 6.** Coupled DSSR; (a) top view on microstrip and (b) lumped equivalent circuit model.

fact of the coupled DSSR structure in Figure 6(a), the parallel shunt capacitor ( $C_P$ ) is increased due to the fringing field, i.e., fringing capacitance. The increased  $C_P$  can instantly be found as 1.17 pF by fitting the circuit simulated resonant pole to the EM simulated one. This explains that  $C_S$  and  $C_P$  of the coupled DSSR can easily be determined by adjusting the bandwidth and resonant pole location, respectively. Thus, the lumped element values of the coupled DSSR for the given dimensions are found as  $C_{DSSR} = 0.014$  pF,  $L_{DSSR} = 1.37$  nH,  $C_P = 1.17$  pF, and  $C_S = 0.14$  pF. The distributed equivalent circuit model of the coupled DSSR is also similar to Figure 3(b). By placing  $C_S$  at  $T_2$  and  $T_2'$  in Figure 3(b), the distributed equivalent circuit model can be obtained. The circuit and EM simulated  $S$ -parameters of the coupled DSSR are shown in Figure 7. The lumped circuit and EM simulated results match well, but the distributed model's resonant frequency shows 90 MHz difference to the EM simulated one. However, the distributed model still provides a reasonable estimation for determining the resonant location of the DSSR.

### 3. TUNABLE DUMBBELL SHAPED SLOT RESONATOR

Figure 8(a) shows the microstrip circuit configuration of the proposed tunable DSSR. In Figure 8(a), DC is isolated from input and output RF ports by coupled gaps ( $G_2$ ). Thus, additional lumped DC block capacitors are not necessary for this tunable resonator. Other gaps ( $S$ ) are also added for an isolation of DC bias in Figure 8(a). By employing the gap ( $S$ ), the series capacitance ( $C_S$ ) due to the coupled gap dimension ( $G_2$ ) is decreased. As a result, the resonant frequency is slightly shifted toward to the high frequency region. However, the

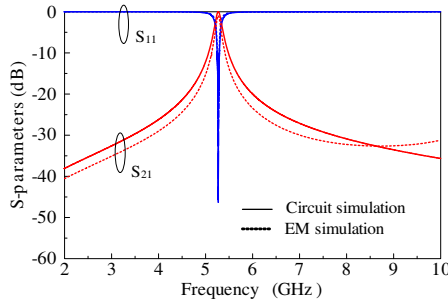


**Figure 7.** Circuit and EM simulated results of the coupled DSSR.

accurate lumped element values for the tunable DSSR can still be determined since their element values are obtained from the simulated  $S$ -parameters. Without a varactor diode, the equivalent circuit model of the tunable DSSR is the same as the one in Figure 6(b). In order to demonstrate the proposed tunable DSSR and its equivalent circuit, the DSSR dimensions in Figure 8(a) are arbitrarily selected as  $D = 4.5$ ,  $G_1 = 0.6$ ,  $G_2 = 0.2$ ,  $P_1 = P_2 = 0.7$ ,  $P_3 = 0.6$ ,  $W = 1.56$ , and  $S = 0.1$  mm. The corresponding lumped element values for the given tunable DSSR dimensions can be determined by using the same method described in the previous section. The exact  $C_{DSSR}$  for  $G_1 = 0.6$  and  $W = 1.56$  mm is found as 0.01 pF from a cross coupled microstrip line modeling. The parallel shunt capacitance ( $C_P$ ) is calculated from (1), and then the series capacitance ( $C_S$ ) is obtained by fitting the circuit simulated pass-band bandwidth to the EM simulated one. As mentioned in Section 2, the coupled DSSR's bandwidth is dominantly affected by  $C_S$  in Figure 6(b). Thus,  $C_S$  can simply be found. After that,  $L_{DSSR}$  is determined by matching the circuit simulated resonant pole location to the EM simulated one. The lumped element values for the given dimensions are  $C_{DSSR} = 0.01$  pF,  $L_{DSSR} = 1.47$  nH,  $C_P = 0.8$  pF, and  $C_S = 0.13$  pF. Figure 8(b) presents the circuit/EM simulated and measured  $S$ -parameters of the tunable DSSR without a varactor diode. As shown in Figure 8(b), the designed tunable DSSR resonates at 6.04 GHz, and its simulated and measured results show good agreement.

The lumped equivalent circuit of the tunable DSSR with a varactor diode is shown in Figure 9. The variable capacitance ( $C_V$ ) due to the different bias condition of the varactor diode changes the resonant frequency of the DSSR. Figures 10(a) and (b) present the simulated and measured  $S_{21}$  for the different bias levels of the varactor diode, where the tunable DSSR dimensions are equal to Figure 8(a).

Thus, the lumped element values in Figure 9 are also the same as  $C_{DSSR} = 0.01$  pF,  $L_{DSSR} = 1.47$  nH,  $C_P = 0.8$  pF, and  $C_S = 0.13$  pF. The varactor diode used for this experiment is MA46600 from M/A-COM. This diode typically provides 0.381 pF with no bias and 0.243 pF with 30 volts. From a diode modeling, the measured diode junction capacitances ( $C_V$ ) have been found as 0.31, 0.295, 0.278, and 0.27 pF for 0, 5, 10, and 15 volts, respectively. The resonant frequency ( $f_0$ ) of the DSSR in Figure 6(b) can be written as (2), where  $C_{Total}$  is the total capacitance of the coupled DSSR without the diode capacitance ( $C_V$ ). Then, the resonant frequency ( $f_R$ ) of the tunable DSSR's equivalent circuit in Figure 9 can be estimated using (3), where  $f_0$  can simply be found from EM simulation. The circuit simulated resonant locations

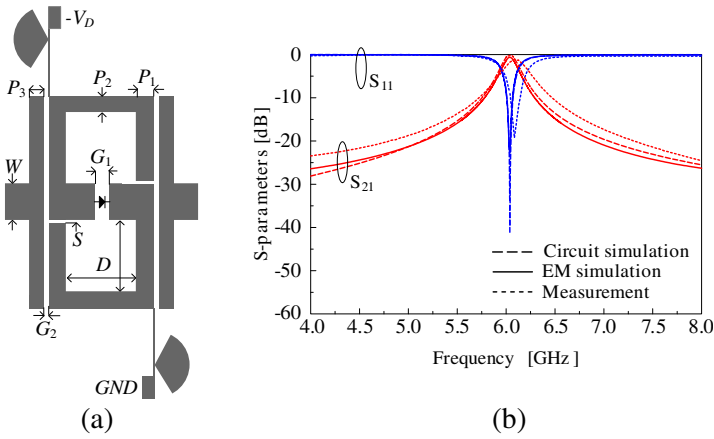


**Figure 8.** Proposed (a) tunable DSSR ( $D = 4.5$ ,  $G_1 = 0.6$ ,  $G_2 = 0.2$ ,  $P_1 = P_2 = 0.7$ ,  $P_3 = 0.6$ ,  $W = 1.56$ , and  $S = 0.1$  mm) and (b)  $S$ -parameter characteristics without varactor diode.

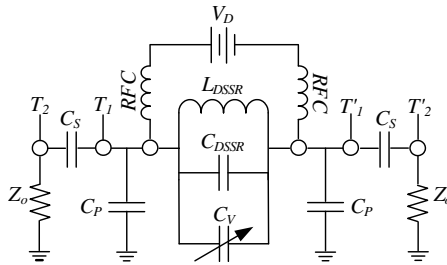


**Figure 9.** Equivalent circuit model of the varactor tuned DSSR.

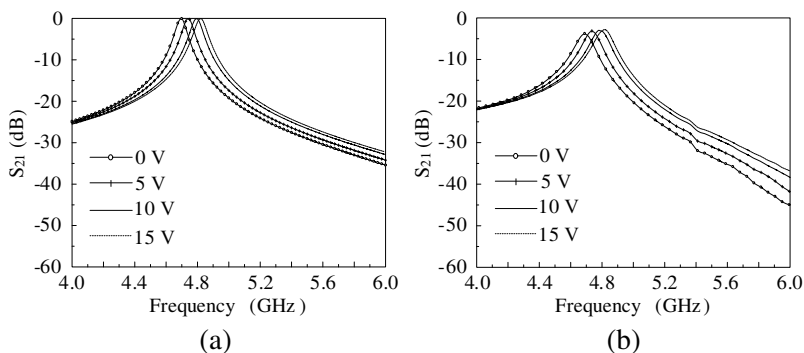


**Figure 10.** Varactor tuned DSSR’s (a) circuit simulated  $S_{21}$  ( $C_{V,0V} = 0.31$ ,  $C_{V,5V} = 0.295$ ,  $C_{V,10V} = 0.278$ , and  $C_{V,15V} = 0.27$  pF) and (b) measured  $S_{21}$ .

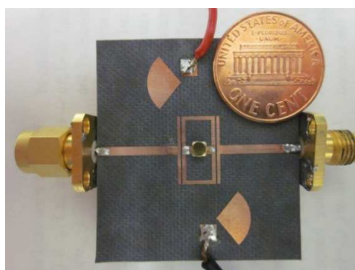


**Figure 11.** Photo of the fabricated tunable DSSR.

in Figure 10(a) show good agreement with the measured results in Figure 10(b). Figure 11 illustrates the photo of the fabricated tunable DSSR.

Quality ( $Q$ ) factor of a microstrip circuit is a strong function of frequency and a substrate thickness [14]. Resonators can be characterized by their unloaded  $Q$  factor ( $Q_U$ ), which is the ratio of the energy stored to the energy dissipated. Since  $Q$  factor is a figure of merit which represents the resonator’s performance, it is an important parameter along with the resonator’s slope parameter. From the measurement, loaded  $Q$  ( $Q_L$ ) can be determined using (4). Once  $Q_L$  is found,  $Q_U$  can also be calculated from (5). Table 1 summarizes the performance of the fabricated tunable DSSR. One important fact in Table 1 is that the tunable DSSR’s  $Q_U$  is a function of varactor diode bias voltage. As the bias voltage increases,  $Q_U$  also increases. This is caused by a diode junction resistance which is in parallel to the

**Table 1.** Resonant frequencies, loaded and unloaded  $Q$  factors of the measured tunable DSSR.

Voltage (V)	$f_R$ (GHz)	$Q_L$	$Q_U$
0	4.69	52.1	144.1
-5	4.74	52.6	170.7
-10	4.79	53.2	182.1
-15	4.82	53.5	188.5

junction capacitance ( $C_V$ ). The junction resistance is dramatically increased, i.e., open circuit, in the reverse bias condition, so  $C_V$  becomes dominant. This junction resistance value is decreased as the diode bias voltage increased. Thus,  $Q_U$  is increased with the diode bias voltage. The unloaded  $Q$  values in Table 1 are in the range of 100 to 200, which agrees with the theoretical calculation for a typical microstrip line [15].

$$f_0 = \frac{1}{2\pi\sqrt{L_{DSSR} \cdot C_{Total}}} \quad (2)$$

$$f_R = \frac{1}{2\pi\sqrt{L_{DSSR} \cdot (C_{Total} + C_V)}} = \frac{1}{\sqrt{\frac{1}{f_0^2} + 4\pi^2 \cdot L_{DSSR} \cdot C_V}} \quad (3)$$

$$Q_L = \frac{\omega_0}{\Delta\omega_{3dB}} \quad (4)$$

$$Q_U = \frac{Q_L}{1 - 10^{[IL(f_R)/20]}} \quad (5)$$

## 4. MINIATURIZED BAND-PASS FILTER DESIGN

### 4.1. Usign Dumbbell Shaped Slot Resonator

In BPF design, the number of filter orders should be considered with the design specifications since it is related to filter's cutoff characteristic. As the number of filter orders increases, the sharper frequency cutoff slope is obtained. However, increasing the filter order also increases an insertion loss due to the dielectric and conduction losses. As illustrated in (5), an insertion loss is the dominant factor to decrease  $Q$ . Thus, one should carefully determine the number of filter orders for a filter design.

Based on the study of the DSSR in Sections 2 and 3, the miniaturized BPF is designed using two coupled DSSRs. The designed BPF using two coupled DSSRs provides the reasonable cutoff slope

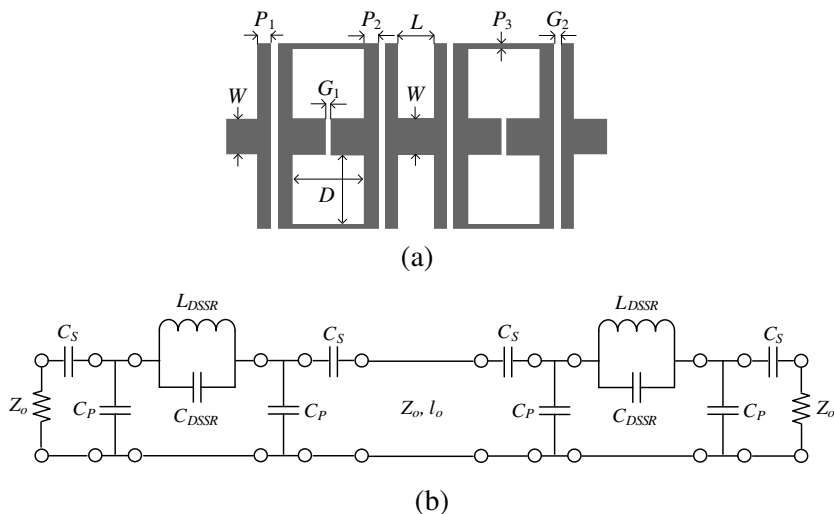


**Figure 12.** The proposed BPF; (a) microstrip circuit configuration and (b) the equivalent circuit model.

and insertion loss. The microstrip circuit configuration of the proposed BPF is presented in Figure 12(a). For the validation of the proposed BPF model, a BPF is designed at the center frequency of 5.8 GHz. In order to design the BPF at the desired center frequency, the dimensions of the single DSSR should be determined. Once the coupled DSSR dimensions resonating at the desired center frequency are obtained, the lumped element values can also be found using the introduced method in the previous sections. After that, the center line length ( $L$ ) is optimized for reasonable insertion and return losses in the pass-band. The characteristic impedance of the center line ( $L$ ) is the same as the input/output port impedances. If the line length ( $L$ ) is decided using circuit simulation, the overall frequency responses of the BPF can be verified using EM simulation. The designed filter dimensions are  $D = 3.93$ ,  $G_1 = G_2 = 0.2$ ,  $L = 3.27$ ,  $P_1 = 0.6$ ,  $P_2 = 0.7$ ,  $P_3 = 0.2$ , and  $W = 1.56$  mm. The equivalent circuit model of the designed BPF is shown in Figure 12(b). The coupled DSSR's equivalent circuits are the same as Figure 6(b), and they are simply connected by a microstrip line with the characteristic impedance of  $Z_o$  and line length of  $l_o$ . Using the proposed technique in Section 2, the lumped element values are found as  $L_{DSSR} = 1.35$  nH,  $C_{DSSR} = 0.22$  pF,  $C_P = 0.97$  pF, and  $C_S = 0.12$  pF. The center line's characteristic impedance is equal to the port impedance, and the line length is optimized as 3.27 mm. The simulated and measured results of the designed BPF are presented

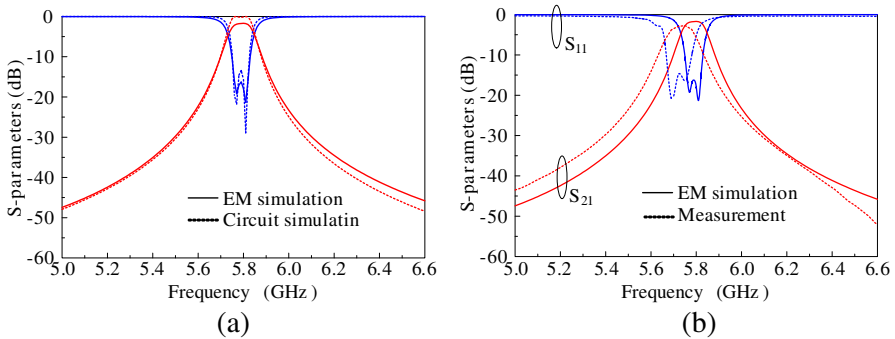


**Figure 13.**  $S$ -parameter comparisons; (a) circuit and EM simulated results and (b) EM and measured results.

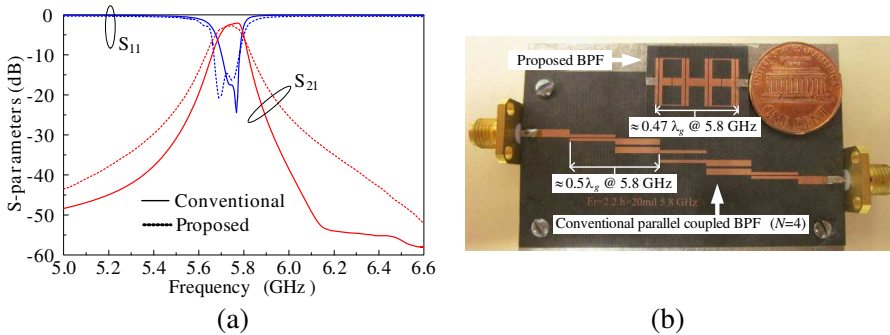


**Figure 14.** Comparisons of (a) measured  $S$ -parameters of conventional parallel coupled BPF and proposed BPF and (b) photo of the fabricated BPFs.

in Figures 13(a) and (b). The circuit and EM simulated results in Figure 13(a) show good agreement, thus the proposed BPF equivalent circuit model in Figure 12(b) is validated. The designed BPF shows the fractional bandwidth ( $FBW$ ) of 0.02, and an insertion loss less than 3 dB in both EM simulated and measured results. Figure 14 presents the comparisons of the proposed BPF and the conventional parallel coupled line BPF. For the comparisons, the parallel coupled line BPF ( $N = 4$ ,  $FBW = 0.02$ ) is fabricated at 5.8 GHz using the same substrate. The measured  $S$ -parameters of both BPFs have been plotted in Figure 14(a). The parallel coupled line BPF with  $N = 4$  shows a steeper cutoff slope than the proposed BPF. However, as shown in Figure 14(b), the proposed BPF has an advantage in size reduction with a reasonable frequency cutoff characteristic.

## 5. CONCLUSION

The microstrip dumbbell shaped slot resonator (DSSR) has been introduced and studied based on a circuit theory and EM simulation. Through an analysis and modeling of the DSSR, the lumped and distributed equivalent circuits have been presented and validated using circuit and EM simulation. As the applications of the DSSR, the tunable DSSR and miniaturized band-pass filter (BPF) are designed, simulated, and measured. In the tunable DSSR design, a varactor diode is simply mounted on the coupled DSSR. The proposed BPF is compact in the dimensions, and provide a sharp frequency cutoff characteristic compared to its size. Since the DSSR is a simple microstrip structure, its analysis and design are relatively easy, and fabrication errors can also be reduced compared to the slotted ground structures.

## ACKNOWLEDGMENT

This work is supported in part by National Science Foundation (NSF) under Grant ECCS-0901088. The author would like to thank Ming-Yi Li, Texas A&M University, College Station, for fabricating the microstrip circuits.

## REFERENCES

1. Chan, K. T., A. Chin, M.-F. Li, D.-L. Kwong, S. P. McAlister, D. S. Duh, W. J. Lin, and C. Y. Chang, "High-performance microwave coplanar bandpass and bandstop filters on Si substrates," *IEEE Trans. Microw. Theory Tech.*, Vol. 51, No. 9, 2036–2040, Sep. 2003.
2. Woo, D. and T. Lee, "Suppression of harmonics in Wilkinson power divider using dual-band rejection by asymmetric DGS," *IEEE Trans. Microw. Theory Tech.*, Vol. 53, No. 6, 2139–2144, Jun. 2005.
3. Liu, H. W., Z. F. Li, X. W. Sun, and J. F. Mao, "An improved 1D periodic defected ground structure for microstrip line," *IEEE Microw. Wireless Compon. Lett.*, Vol. 14, No. 4, 180–182, Apr. 2004.
4. Ahn, D., J. S. Park, C. S. Kim, J. Kim, Y. Qian, and T. Itoh, "A design of the low-pass filter using the novel microstrip defected ground structure," *IEEE Trans. Microw. Theory Tech.*, Vol. 49, No. 1, 86–93, Jan. 2001.

5. Jung, D.-J. and K. Chang, "Low-pass filter design through the accurate analysis of electromagnetic-bandgap geometry on the ground plane," *IEEE Trans. Microw. Theory Tech.*, Vol. 57, No. 7, 1798–1805, Jul. 2009.
6. Balalem, A., A. R. Ali, J. Machac, and A. Omar, "Quasi-elliptic microstrip low-pass filters using an interdigital DGS slot," *IEEE Microwave and Wireless Component Lett.*, Vol. 17, No. 8, 586–588, Aug. 2007.
7. Ting, S.-W., K.-W. Tam, and R. P. Martins, "Miniaturized microstrip lowpass filter with wide stopband using double equilateral U-shaped defected ground structure," *IEEE Microwave and Wireless Component Lett.*, Vol. 16, No. 5, 240–242, May 2006.
8. Chen, J., Z.-B. Weng, Y.-C. Jiao, and F.-S. Zhang, "Lowpass filter design of Hilbert curve ring defected ground structure," *Progress In Electronmagnetics Research*, Vol. 70, 269–280, 2007.
9. Wang, X.-H., B.-Z. Wang, and K. J. Chen, "Compact broadband dual-band bandpass filters using slotted ground structure," *Progress In Electronmagnetics Research*, Vol. 82, 151–166, 2008.
10. Lim, J.-S., Y.-T. Lee, C.-S. Kim, D. Ahn, and S. Nam, "A vertically periodic defected ground structure and its application in reducing the size of microwave circuits," *IEEE Microwave and Wireless Component Lett.*, Vol. 12, No. 12, 240–242, Dec. 2002.
11. Park, J.-S., J.-S. Yun, and D. Ahn, "A design of the novel coupled-line bandpass filter using defected ground structure with wide stopband performance," *IEEE Trans. Microwave Theory and Tech.*, Vol. 50, No. 9, 2037–2043, Sep. 2002.
12. Kim, C.-S., D.-H. Kim, I.-S. Song, K. M. K. H. Leong, T. Itoh, and D. Ahn, "A design of a ring bandpass filters with wide rejection band using DGS and Spur-line coupling structures," *IEEE MTT-S Int. Microwave Symp. Dig.*, 2183–2186, Jun. 2005.
13. Kwok, S. K., K. F. Tsang, and Y. L. Chow, "A novel capacitance formula of the microstrip line using synthetic asymptote," *Microw. Opt. Technol. Lett.*, Vol. 36, No. 5, 327–330, Mar. 2003.
14. Chnag, K., *Microwave Solid-state Circuits and Applications*, Wiely, 1994.
15. Gopinath, A., "Maximum  $Q$ -factor of microstrip resoantors," *IEEE Trans. Microw. Theory Tech.*, Vol. 29, No. 2, 128–131, Sep. 1981.